## 4 Remote Sensing and GIS Investigation

### 4.1 General Background

The term "Remote Sensing" refers to methods that employ electromagnetic energy, such as light, heat and radio waves as the means of detecting and measuring target characteristics (Sabins, 1987). Remote sensing can provide information for large areas, and in a relatively short time. In addition, remote sensing is not limited by extremes in terrain or hazardous condition. Generally, remote sensing should be integrated into early stages of investigations and be used in conjunction with traditional mapping techniques.

Remote sensing data were used in this study for the following purposes:

1. to preliminary assess or characterize the study area to support data and to target areas for traditional assessment techniques such as field mapping and geophysical investigation;
2. to clarify the geoscientific problems that can be solved more effectively with the general overview provided by satellites and airplanes.

There were many attempts to use the remote sensing data and its techniques to detect the salt-affected soil. Some of these studies are summarized below:

Multispectral scanning (MSS) technology for natural resources surveys is used in the images obtained by Landsat MSS and TM (Thematic Mapper) as well as SPOT. Type and variation of the images depend on the scanners, which record the reflected radiations in the separate bands. Landsat offers a wider range of bands (spectral diversity) than SPOT, which enhance the detection of surface features.

Dwivedi (1969) applied principle component analysis of Landsat MSS bands 1, 2, 3 and 4 in delineating salt affected soils.

Chaturvedi *et al.* (1983) and Singh & Srivastava (1990) employed satellite data for salinity detection by using microwave brightness and thermal infrared temperature synergistically. The interpretation of the microwave signal was done by means of a two-layer model with fresh and saline groundwater.

Menenti, Lorkeers & Vissers (1986) found that TM data in band 1 through band 5 and band 7 are good for identifying salt minerals, at least when salt is a dominant soil constituent. Moreover, salt minerals affect the thermal behavior of the soil surface.

Mulders & Epema (1986) produced thematic maps indicating gypsiferous, calcareous and clayey surface using TM band 3, 4 and 5. They found TM data a valuable aid for mapping soil in arid areas when used in conjunction with aerial photographs.

Sharma & Bhargava (1988) followed a collative approach comprising the use of Landsat 2 MSS "FCC" or False Color Composite, survey of topographic maps and limited field checks for mapping saline soils and wetlands. Their results showed that because of their distinct coloration and unique pattern on false color composite imageries the separation of saline and waterlogged soil is possible.

Saha, Kudart, & Bahn (1990) used digital classification of TM data in mapping salt affected and waterlogged land in India, and found that these salt-affected

and waterlogged areas could be effectively delineated, mapped and digitally classified with an accuracy of about 96 percent using bands 3, 4, 5 and 7.

Rao *et al.* (1991) followed a systematic visual interpretation approach using the False Color Composite of TM bands 2, 3 and 4 for mapping two categories, moderately and strongly sodic soils.

Brena *et al.* (1995) used multiple regression analysis of the electrical conductivity values and spectral observations to estimate the electrical conductivity for each pixel in the field, based on sampling sites in Mexico. They generated a salinity image using the regression equation.

Naseri (1998) suggested that both types of digital classification, unsupervised and supervised, could be used for the proper identification of salinity, mostly at a regional level. MSS bands 3, 4 and 5 are recommended for salt detection in addition to TM bands 3, 4, 5 and 7.

Fouad (2003) applied ASTER bands 3, 4 and 5 data in terms of a salinity index together with the biophysical method based on detecting the crop reaction to soil salinity via osmotic forces and the increasing surface resistance due to stomatal closure to detect salinity in the irrigated area in the northern part of Syria.

In Thailand, remote sensing technology was first adopted and used for military and land use mapping and later for the natural resources exploitation purposes. These techniques were first used to generate, classify and map saline soil in northeastern Thailand by the Land Development Department (LDD) in 1975, and later revised in 1981 and 1989.

Sinanuwong *et al.* (1980) described the application of Landsat imagery of July 1975 and 1976 coupled with ground sampling in about 2 000 km2 of the Nakhon Ratchasima Province. The soil salinity classes were arbitrarily divided into areas of non-, slightly, moderately and strongly salt-affected, based on the interpretation of the imagery.

Arunin *et al.* (1981) and (1984) used aerial photographs and Landsat MSS data to detect and study the characteristics of saline soils in northeastern Thailand. They also compared the soil salinity map produced in 1975 to a soil salinity map of 1981. They found that the salt-affected areas increase of 36 percent and the degree of salinization increased in all classes.

Limpinuntana & Arunin (1986) estimated based on satellite imagery, that there are 2.85 M ha of salt-affected soils in northeast Thailand or about approximately 17 per cent of the total area. These saline areas can be subdivided into three classes; slightly, moderately and severely salt-affected areas. They also show another 10.8 M ha being potentially saline.

Eiumnoh *et al.* (1994) developed a methodology to classify the salt-affected soils using remote sensing combined with GIS. Their study area was Nakhon Ratchasima Province, Thailand. Supervised classification was employed with maximum likelihood, Mahalonobis and minimum distance methods on the Landsat TM bands 1, 3, 4, 5 and 7. Unsupervised classification was also tried with sequential clustering resulting in seven separable classes. A similar pattern of soil salinity was obtained from the study compared to the existing LDD's map in 1989.

Sukchan *et al.* (2000) used Landsat 5 TM integrated with GIS for improvement of classification methods to detect salt-affected areas in Northeast

Thailand. They found that the operation of dividing areas according to soil type and landform information derived from map data could lead to a reliable classification with an overall accuracy of 85.26 percent of their salt-affected areas classification.

Khundee (2003) combined and overlaid the soil salinity maps of LDD with lineaments derived from Landsat TM and MOMS imagery to clarify the relationship between salinity and tectonic processes.

## 4.2 Remote Sensing Data Used

Remote sensing data used in this study were taken by different satellite observation systems. The data were purchased by the Thai-German Environmental Geology Project and are available at BGR and DMR in the form of CD-ROMs. The remote sensing data employed in this study consist of the following observation systems:

1) Landsat 5 (TM) and Landsat 7 (ETM+),
2) ASTER,
3) SRTM.

### 4.2.1 Landsat 5 (TM) and Landsat 7 (ETM+) Data

Landsat satellites have been collecting multispectral images of the Earth's land surface since the 1970's. This unique data archive has played an important role across disciplines as a tool used toward achieving improved understanding of the Earth's land surface impacts on the environment. The purpose of the Landsat program is to provide the world's scientists and application engineers with a continuing stream of remote sensing data for monitoring and managing the Earth's resources. Landsat 7 (ETM+) is the latest NASA satellite in a series that has produced an uninterrupted multispectral record of the Earth's land surface since 1972. The main parameters of the Landsat 5 (TM) and Landsat 7 (ETM+) data are summarized in Table 4.1.

Table 4.1 Parameters of Landsat 5 (TM) and Landsat 7 (ETM+) data.

| | Landsat 5 (TM) | Landsat 7 (ETM+) |
|---|---|---|
| Spectral bands | Band 1: 0.45 - 0.52 μm (VIS) | Band 1: 0.45 - 0.52 μm (VIS) |
| | Band 2: 0.52 - 0.60 μm (VIS) | Band 2: 0.52 - 0.60 μm (VIS) |
| | Band 3: 0.63 - 0.69 μm (VIS) | Band 3: 0.63 - 0.69 μm (VIS) |
| | Band 4: 0.76 - 0.90 μm (NIR) | Band 4: 0.76 - 0.90 μm (NIR) |
| | Band 5: 1.55 - 1.75 μm (SWIR | Band 5: 1.55 - 1.75 μm (SWIR |
| | Band 7: 2.08 - 2.35 μm (SWIR) | Band 6: 2.08 - 2.35 μm (SWIR) |
| | Band 6: 10.40 - 12.50 μm (TIR) | Band 7: 10.40 - 12.50 μm (TIR) |
| | | Band 8: Panchromatic |
| Orbit altitude | 705 km | 705 km |
| Swath width | 170 km (170 km x 185 km standard image size) | 170 km (170 km x 185 km standard image size) |
| Pixel size (GIFOV) | 30 m (VIS/NIR/SWIR) | 30 m (VIS/NIR/SWIR) |
| | 120 m (TIR) | 60 m (TIR) |
| | | 15 m (Pan) |

The data sets of Landsat 5 (TM) and Landsat 7 (ETM+) that have been evaluated and interpreted for the study area as shown in Table 4.2.

Table 4.2 Landsat 5 (TM) and Landsat 7 (ETM+) Satellite data used in this study.

| System | Data Acquisition Date | Path/Row | Comments/Quality |
|---|---|---|---|
| Landsat 5 | 25 April 1994 | 128/049 | Partly covered by dust |
| Landsat 5 | 06 March 1999 | 128/049 | High quality, no cloud cover |
| Landsat 5 | 06 March 1999 | 128/050 | High quality, no cloud cover |
| Landsat 5 | 06 March 1999 | 128/49/50 fl. | High quality, no cloud cover |
| Landsat 7 | 27 December 1999 | 128/049 | good High quality, no cloud cover quality, no cloud cover |
| Landsat 7 | 27 December 1999 | 128/050 | good quality, no cloud cover |
| Landsat 7 | 13 February 2000 | 128/049 | High quality, no cloud cover |
| Landsat 7 | 13 February 2000 | 128/050 | High quality, no cloud cover |
| Landsat 7 | 03 May 2000 | 128/049 | Partly dusty, showing standing water |
| Landsat 7 | 03 May 2000 | 128/050 | Partly dusty, showing standing water |

### 4.2.2 The Advanced Space borne Thermal Emission and Reflection Radiometer (ASTER)

The Advanced Space borne Thermal Emission and Reflection Radiometer (ASTER) is an advanced multispectral imager that was launched on board NASA's Terra spacecraft in December 1999. ASTER covers a wide spectral region with 14 bands from visible to the thermal infrared with a high spatial, spectral and radiometric resolution. An additional backward-looking near-infrared band provides stereo coverage.

ASTER consists of three different subsystems: the Visible and Near-Infrared (VNIR) has three bands with a spatial resolution of 15 m, and additional backward telescope for stereo coverage; the Short-Wave Infrared (SWIR) has 6 bands with a spatial resolution of 30 m, and the Thermal Infrared (TIR) has 5 bands with a spatial resolution of 90 m. Each subsystem operates in a different spectral region and with its own telescopes. Each ASTER scene covers a 60 x 60 km.

In this study 5 scenes ASTER Level -1A data were employed. ASTER Level-1A data are formally defined as reconstructed, unprocessed instrument data at full resolution. They consist of the image data without applying the corrections to the image data, thus maintaining original data value. The ASTER Level-1A data, which cover the study area, and used in this study were acquired on November 21, 2001, December 7, 2001, January 17, 2002, and 2 scenes with different scene centers in February 2, 2002, respectively.

The comparison of spectral bands between ASTER and Landsat 7 is shown in Table 4.3 and Figure 4.1 respectively.

Table 4.3 Spectral bands and the resolution of ASTER and Landsat data.

| ASTER | | | | Landsat-TM | | |
|---|---|---|---|---|---|---|
| | Band Number | Spectral range (μm) | Spatial resolution (m) | Band Number | Spectral range (μm) | Spatial resolution (m) |
| VNIR | | | | 1 | 0.45 – 0.52 | |
| | 1 | 0.52 – 0.60 | | 2 | 0.52 – 0.60 | |
| | 2 | 0.63 – 0.69 | 15 | 3 | 0.63 – 0.69 | |
| | 3 | 0.76 – 0.86 | | 4 | 0.76 – 0.90 | |
| SWIR | 4 | 1.60 -1.70 | | 5 | 1.55 – 1.75 | 30 |
| | 5 | 2.145 – 2.185 | | | | |
| | 6 | 2.185 – 2.225 | | | | |
| | 7 | 2.235 – 2.285 | 30 | 7 | 2.08 – 2.35 | |
| | 8 | 2.295 – 2.365 | | | | |
| | 9 | 2.360 – 2.430 | | | | |
| TIR | 10 | 8.125 – 8.475 | 90 | | | |
| | 11 | 8.475 – 8.825 | | | | |
| | 12 | 8.925 – 9.275 | | | | |
| | 13 | 10.250 – 10.950 | | 6 | 10.4 – 12.5 | 60 (ETM7) |
| | 14 | 10.950 – 11.650 | | | | 120 (TM5) |

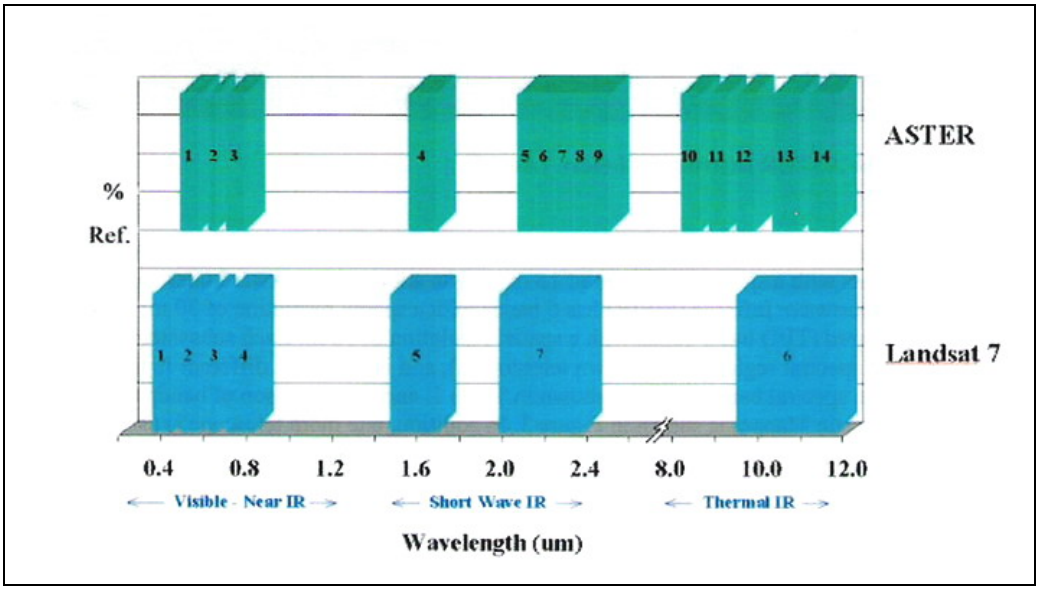


Figure 4.1 Comparison of spectral bands between ASTER and Landsat 7 (ETM+) (Note: % Ref is reflectance percent) (ASTER user handbook, Jet Propulsion Laboratory/California Institute of Technology)

### 4.2.3 The Shuttle Radar Topography Mission (SRTM)

The Shuttle Radar Topography Mission (SRTM) is a joint project between the National Imagery and Mapping Agency (NIMA) and the National Aeronautics and Space Administration (NASA). The objective of this project is to produce digital

topographic data for 80% of the Earth's land surface. SRTM makes use of the radar interferometry technique. In radar interferometry, two radar images are taken from slightly different locations. Differences between these images allow for the calculation of surface elevation, or change. The spatial resolution of SRTM is 90 m. SRTM data, which cover the study area, between longitudes 101o00' and 102o00'E, and latitudes 14o00' and 16o00'N, is employed in this study as a digital terrain model to further study how the topography characteristics of the study area are related to the occurrence of salinity.

## 4.3 Image Processing

Image processing is applied to compensate data errors and geometric distortions, to enhance and extract features related to thematic subjects being under investigation and to suppress redundant information. In this study, standard tools of image processing have been used for digital processing of the satellite data. Digital image processing was used to

- register the originally orbit oriented raster data over the UTM coordinates system
- enhance and to extract features that indicate targets of interest in the data.

In this study, the digital image processing processes were conducted in the following steps:

### 4.3.1 Image Registration (Geo-referencing)

Registration is the process of superimposing an image over a map or over another already registered data. The method of image registration or "geo-referencing" can be divided into two types: "image-to-image-registration" and "image-to-map-registration". Selected image data of the Khorat area was rectified with reference to the 1:50 000 scale topographic maps (image-to-map-registration). Further imagery was geo-referenced to this already registered satellite image using the image-to-image registration.

Landsat 7 acquired on December 27, 1999 and ASTER acquired on December 7, 2001, images were defined as the master images for the registration. They were registered using image-to-map geo-referencing techniques with reference to the Thai-Vietnam Datum, UTM, Zone 48, Thai/Vietnam datum (the areas overlapping with UTM Zone 47 were converted to Zone 48). The topographical base was the official 1:50 000 scale topographic map series published by the Royal Thai Survey Department of Thailand. The major steps of image registration are:

#### a) Selection of the Ground Control Points (GCPs)

The GCPs were collected from 1:50 000 topographic maps of Maung Chaiyaphum, Khon Sawan, Phon, Jaturat, Ban Laum, Bua Yai, Prathai, Nong Song Hong, Nong Bua Kok, Kham Sakae Saeng, Khong, Chum Puang, Ban Kra Beaung, Dan Khun Thot, Non Thai, Non Sung, Ban Phut Sa, Lam Plai Mas, Sung Neon, Maung Nakhon Ratchasima and Ban Sa Ra Phi area. GCPs are landmarks, which are identifiable both

on the image and on the map. Landmarks for image registrations are cross-roads, bridges and railroad crossing. However, because of the insufficient correspondence of the map road net, and the actually existing road net and the topographic base maps not being up to date, it has been very difficult to cover the image with well-distributed and precise GCPs.

**b) Implementation of the registration and warping procedure**

The warping procedure is the computing of an affine projection that links the image and the map coordinate systems with an interpolation of the data (nearest, bilinear, cubic interpolation). For the warping procedure, the image processing software ENVI 3.4 was employed to establish least squares polynomial equations to link the image coordinates (row/line-based) to the map coordinates. Reference points are the GCPs. This process primarily performs a rotation of the scene with the respect to grid north (warping) in order to adjust the pixel-raster of the scene to the map grid.

Normally, registration is performed by changing the locations and the size of the original pixels. Interpolation and resampling methods are applied to calculate the corresponding positions and the digital number values (DN) of the pixels in the output image. In this study the polynomial warping of 1st degree has been applied to compute an affine projection to link the image and the map coordinate systems. Bilinear interpolation has been applied to compute the digital number (DN) values in the warped image. Bilinear interpolation uses the surrounding 4 pixels values from the older grid. As result of image registration, each pixel of the satellite image is assigned with a pixel coordinate and a UTM coordinate as well.

### 4.3.2 Image Enhancements

Image enhancement is the modification of an image in order to alter its impact on the viewer (Sabins, 1987). Generally, image enhancement changes the original digital value and it should be carried out after geo-referencing. The purpose of image enhancement is to make the images more interpretable for specific applications. The general aim of image enhancement is to highlight features of thematic interest (lineament, rock and soil properties, etc.) and to suppress redundant information.

Major tools applied for the enhancement of the Khorat Basin satellite data were histogram analysis and contrast stretching, edge enhancement, Band Ratioing, RGB-Coding and Principal Component Transformation.

### 4.3.3 Image Mosaicking

ENVI 3.4 software was employed to mosaic the satellite images, which cover the study area by using a geographical mosaicking method. The aim is to generate new images which cover the study area located between longitudes 101o30’ and 102o30’ E, and latitudes 14o45’ and 16o00’ N. For Landsat data, the raw data of the Landsat 7 data acquired on December 27, 1999 with Row 128/Path 49 and 50 are mosaicked to each other. For ASTER data, the raw data of the data acquired on November 21, 2001, December 7, 2001, and 2 scenes with different scene center of February 22, 2002 were mosaicked all together.

## 4.4 Lineament Analysis

A lineament is any extensive linear surface on a planet, as a fault line or fracture line. The term “lineament” is one of the most commonly used terms in geology. Hobbs (1904) first used the term lineament to define a “significant line of landscape which reveals the hidden architecture of rock basement”. Gupta (1991) summarized the definition of lineament in different geological features, such as (1) shear zones/faults; (2) rift valleys; (3) truncation of outcrops; (4) fold axial traces; (5) joint and fracture traces; (6) topographic, vegetation, soil tonal changes alignment, etc. Lineaments are commonly interpreted as surface expressions of rock fractures which may provide pathways for upward transport of groundwater from subsurface.

In Northeastern Thailand, on terrace and basin areas lineaments show up by the high reflection of dry weathered soil along its trends. The weathering process of rocks starts along lineaments, especially in non-competent sediments (shale, clay, sandy clay or rock that clay is predominant) interbedded with competent rocks (sandstone).

From satellite images it can be observed that the combination of processes such as capillary phenomena, water run off, salt solution etc., produces salt contamination and dissolution feature near or at surface. When saline moisture contaminates near or at surface, the reflection from saline moisture can be detected by satellite sensor. Malila (2002) called this kind of lineament feature “salt lineament trace”. Most of the detected sites are located on younger sediment of Tertiary age.

Fractures and joints occur in a wide variety of rock types and tectonic environments. Archvichai (1989) and Chuaviroj (1997) postulate that fractures and joints in this area are associated with regional folding and salt tectonics. The regional folding formed anticlines and synclines with fractures and joints within the salt and overburden structures. Its forming was due to compression and tension. In folded strata radial fractures were formed by a tension and extension mechanism (Warren, 1999). Axial plane cleavage (fractures and joints) developed during folding. On images, fractures and joints are short distance linears (up to 3 km) and cross prominent lineaments in the central, northern and western part of the study area.

Another major type of lineaments found in the Korat Plateau is the contact between Khok Kruat Formation and Maha Sarakham Formation. Especially formations bearing rock salt and formations without rock salt show prominent boundaries due to their differential weathering level. Normally, the formation bearing rock salt is less resistant than the overlying the Phu Tok Formation, which consists of siltstone, claystone and sandstone. Therefore the area occupied by a formation bearing salt forms low land. Some parts of this will develop streams, which are parallel to the more elevated land of the Phu Tok Formation. Rock boundary lineament are found in Waeng Yai, Waeng Noi, west of Dan Khun Thot, north of Chaiyaphum Province, and south and southeast rim of Nakhon Ratchasima district area.

As mentioned above, salt may be brought up to the surface by groundwater especially from deeper levels. The study of both the quantity and characteristics of a lineament is one of the most important factors to indicate areas, where soil or water could be salinized. The aim of lineament analysis from satellite data is to locate the potential salt-affected areas by using the intensity and orientation of the lineaments as clue.

### 4.4.1 Previous Work on Lineament Analysis in the Khorat Plateau

Jantaranipa *et al.* (1981) reported that the relationship of major and minor lineaments, lineament density contours, lineaments intersection density contours can indicate mineral zones.

Supajanya (1992) showed in his investigation collapsed sinkholes as a promising source for shallow groundwater in the rural areas in Northeastern Thailand. His study indicated that the collapsed sinkholes distributions are associated with joint patterns within the region.

Thanomsap (1992) presented an analysis of lineaments interpreted from Landsat imagery. He first traced lithology boundaries, folds and faults and then extracted lineaments from topographic relief and/or tonal differences. The lineament map was divided into 5 sections; the Paleozoic province, the Sakon Nakhon Basin province, the large Anticline area or Phu Phan Anticlinorium, the Khorat Basin and the Petchabun Basin, based on lineament pattern and geological setting for the purpose of optical analysis.

Chuaviroj (1997) studied the deformation in the Khorat Plateau by Landsat TM satellite images and aerial photographic interpretation. He recognized 3 episodes of deformation in Mesozoic rocks as described in section 2.4 (structural framework).

### 4.4.2 Methodology

#### a) Lineament Information and Data Source Collection

The data set used for this analysis is Landsat 7 image recorded on December 27, 1999 (Row 128/Path 49 and 50) because it is of good quality and shows less cloud covered than others. The data was loaded and processed on a workstation using ENVI 3.4 and Geomatica image processing software. The lineaments have been analyzed after enhancing and stretching the contrast. The traces of lineaments were then visually interpreted and drawn on transparent overlays on the plotted images.

#### b) Data Processing and Image Products

Following a number of processing techniques (Jensen, 1986 and Mather, 1987), the contrast of six bands data of the Landsat imagery was digitally enhanced. The images of all bands were compared in term of contrast and geological features (lineaments). As a result of visual evaluation, Landsat 7 band 3 data, which record the information at the wave-length between 0.63-0.69 nm (VIS) were selected for this study, since it shows good contrast and displays geological lineaments compared to the other bands. After a lot of trials and errors to find a suitable combination of 3 bands for lineament analysis, the False Color Composite Landsat 7 acquired on December 27, 1999, bands 4, 3, 2 as red, green, blue shows the sharp lineament traces best for visual interpretation. The single Landsat band 3 and a False Color Composite Landsat 7 acquired on December 27, 1999, bands 4, 3, 2 as red, green, blue which were used as based images for lineament analysis are shown in Figure 4.2 and Figure 4.3, respectively.

In order to enhance the structural geological information (lineaments) further, filtering techniques were applied to this Landsat 7 band 3 data. The result shows that a number of filters of the following values produced very good images enhancing the lineaments in the study area. The filter values area as follows:

a) Non-directional filter (Laplacian convolution filter)

| | | |
|---|---|---|
| 0 | -1 | 0 |
| 1 | 5 | -1 |
| 0 | -1 | 0 |

b) Directional filter

N-S

| | | |
|---|---|---|
| 1 | 0 | 1 |
| 2 | 0 | 2 |
| 1 | 0 | 1 |

E-W

| | | |
|---|---|---|
| -1 | -2 | -1 |
| 0 | 0 | 0 |
| 1 | 2 | 1 |

NE-SW

| | | |
|---|---|---|
| 2 | -1 | 0 |
| 1 | 0 | 1 |
| 0 | 1 | 2 |

NW-SE

| | | |
|---|---|---|
| 0 | -1 | -2 |
| 1 | 0 | -1 |
| 2 | 1 | 0 |

Thus, the following images were used in this study:

1. Image of Landsat 7 band 3 with digitally enhanced contrast;
2. Image of Landsat 7 band 3 filtered by a Laplacian convolution filter;
3. Image of Landsat 7 band 3, each one filtered by directional filter N-S, E-W, NE-SW and NW-SE, respectively;
4. The False Color Composites Landsat 7 bands 4, 3, 2 as red, green, blue.

Some of the lineaments are only seen in a certain directional filtered images.
This phenomenon possibly occurs because of artifacts produced by the processing techniques that were applied to the images. To avoid the mistake of considering the artifacts as lineaments, the following methods are followed:

- All lineaments in Landsat 7 band 3 image (contrast enhanced), Landsat 7 band 3 (Laplacian filtered), each of Landsat 7 band 3 filtered by directional filter N-S, E-W, NE-SW and NW-SE, and the False Color Composites of Landsat 7 bands 4,3,2 as red, green, blue were traced separately. All tracings were overlapped, and the lineaments which were presented in all tracings were traced again in the separate tracing.
- A similar method was applied to all images, and only lineaments presented or repeated on at least 3 images were considered for analysis and later mapping.

The lineaments which are more than 5 km long were interpreted to represent faults since they are too big to represent fractures or joints without any displacement that took place along their planes. The results of lineament analysis and its interpretation are shown and later discussed in details in Chapter 6.

### 4.5 Drainage Pattern Analysis

Since the drainage pattern can reflect subsurface geological conditions and rock types, a drainage pattern analysis was also conducted in this study. Most of the rivers and streams are developed on weak zones like fractures, faults or fissures where saline groundwater can migrate to the surface. Therefore, drainage pattern analysis is also important as it is a hint to predict the location of potential areas of salinization. For that purpose, a Principal Component Analysis was conducted and applied to the Landsat 7 data to produce a more layers for false color composite combinations and getting the proper FCC images for drainage pattern analysis. After a lot of trials and errors, the False Color Composites Landsat 7 acquired on December 27, 1999, bands PC1, 5, 3 as red, green, blue was selected for tracing the drainages of the study area since this type of False Color Composite shows a very well traceable drainage network as compared to other False Color Composite images. The Landsat 7 image acquired on December 27, 1999, bands PC1, 5, 3 as red, green, blue is shown in Figure 4.4. The results of drainage pattern analysis are shown and discussed in detail in Chapter 6.

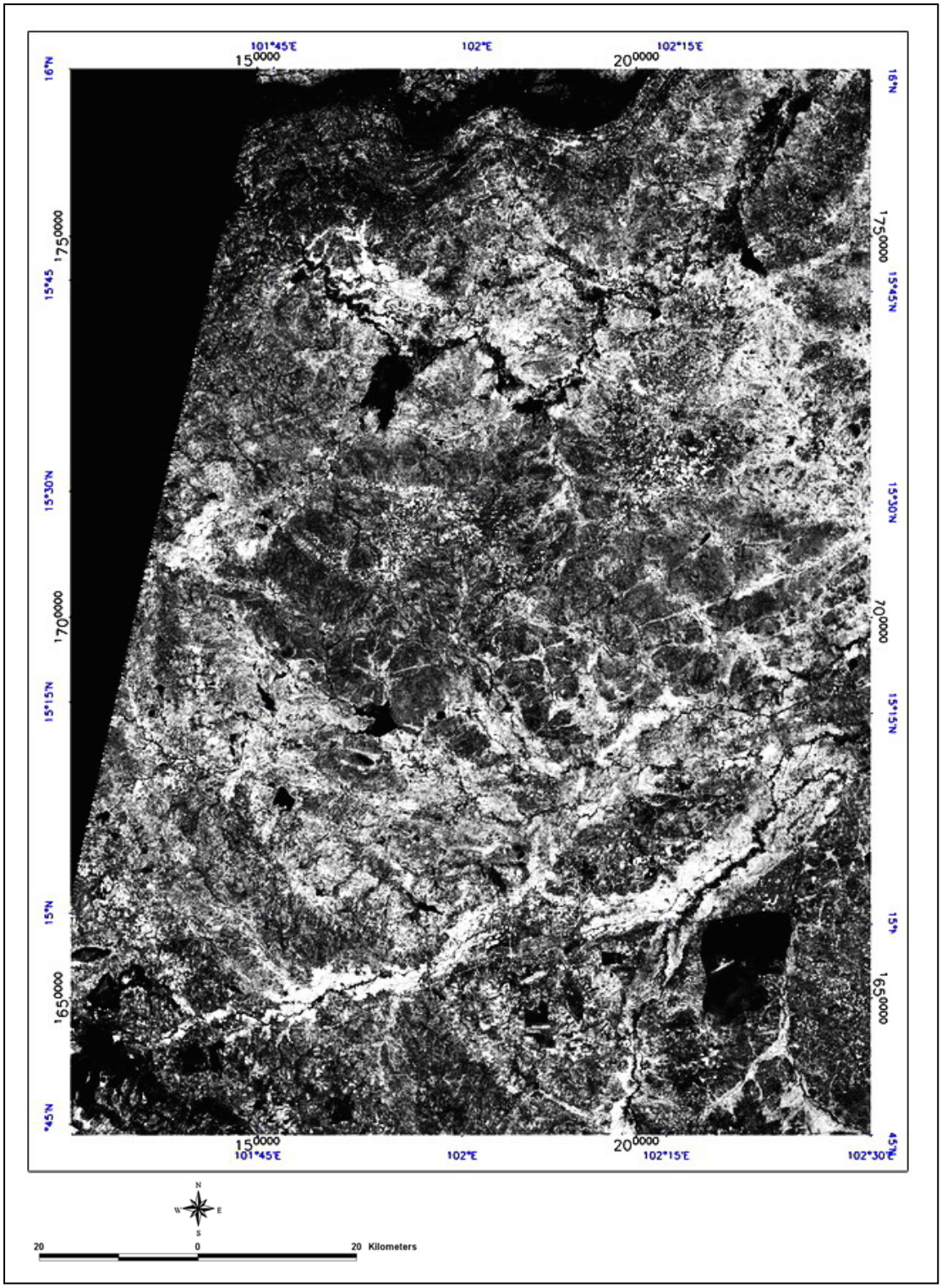


Figure 4.2 The Landsat 7 band 3 acquired on December 27, 1999 which is used as based images for lineament analysis.

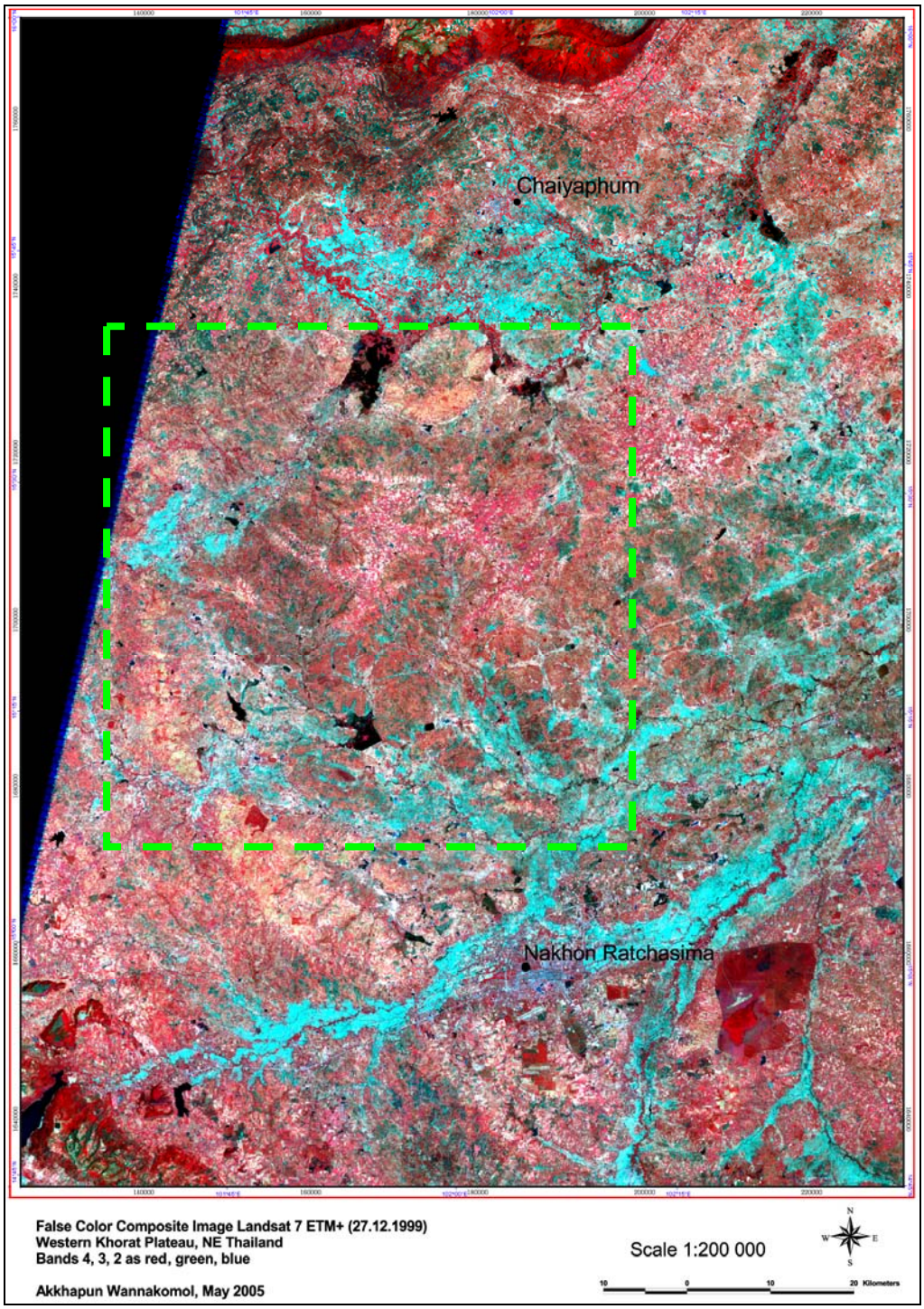


Figure 4.3 The False Color Composites image of Landsat 7 acquired on December 27, 1999, bands 4, 3, 2 as red, green, blue, which was used for lineament, salinity index and vegetation index analysis. Red color represents vegetation, black color represents water bodies, light blue color represents paddy fields, and white color represents saline areas, respectively. The green rectangle showing the covering ASTER data scene used in this Study. (See Enclosure 1 for the full size image)

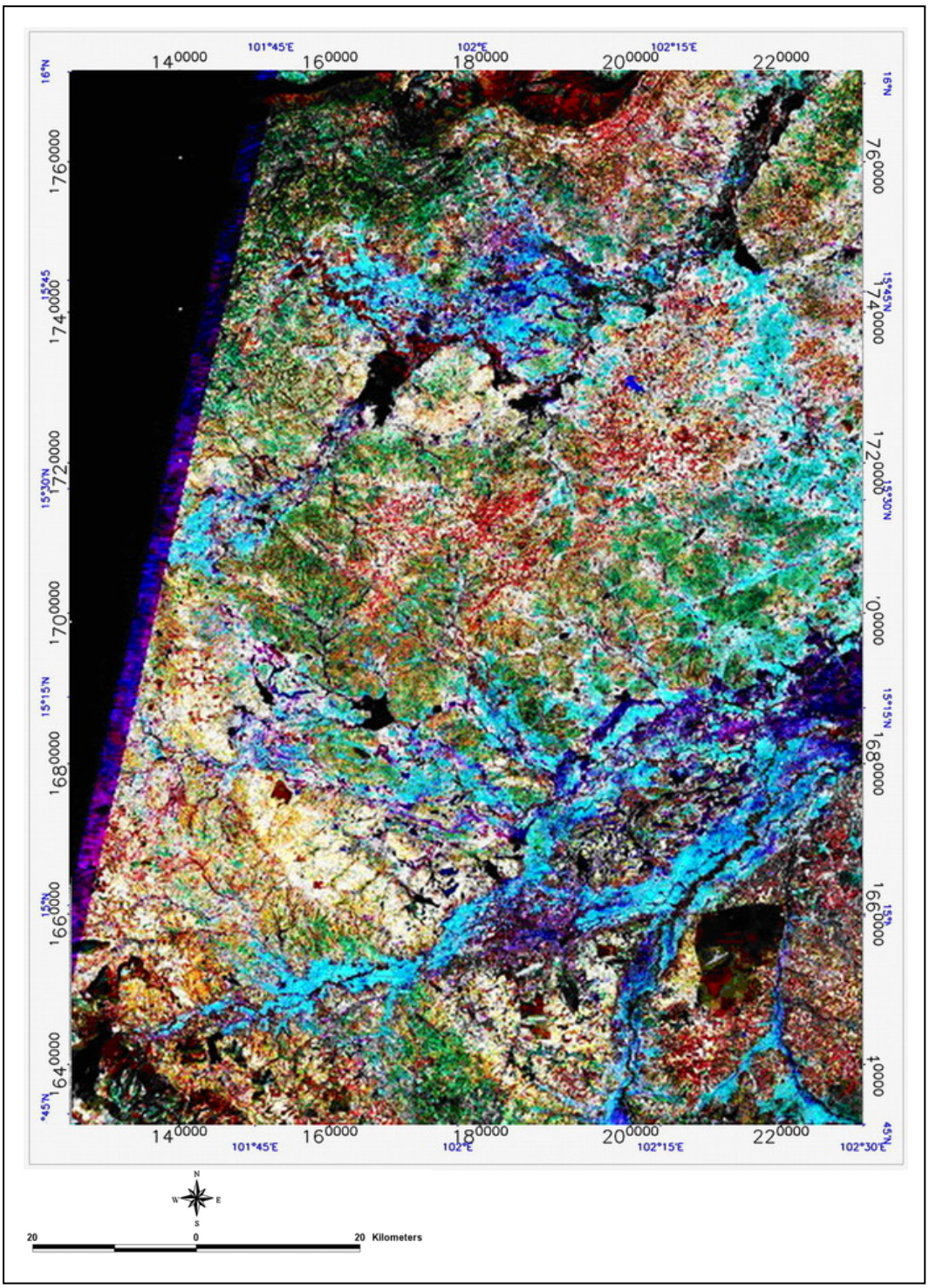


Figure 4.4 The False Color Composites image of Landsat 7, acquired on December 27, 1999, bands PC1, 5, 3 as red, green, blue which was for drainage analysis. Red/yellow color represents dry vegetation, green color represents healthy vegetation, black/dark blue color represents water bodies, light blur color represent paddy fields, and white color represents saline areas, respectively.

## 4.6 Saline Soil Mapping

The problem of detecting, monitoring and mapping salt-affected soils is known to be a difficult matter, since salinization is a dynamic process. The approach to delineate saline soil using remote sensing data and GIS techniques has been proved in many recent studies to be most efficient (Sharma & Bhargava, 1988, Rao et al., 1991, Srivastava et al., 1997, Dwividi et al., 1998). This part of the study aims to differentiate the salt-affected area from non salt-affected areas using various methods of digital image classification and band math methods. To reach that objective, land use was classified using both unsupervised and supervised techniques applied to the Landsat 7 and ASTER data coupled with ground truth investigation to verify the percentage of classification accuracy and to investigate the topographic and other related characteristics of the salt-affected area and those of non salt-affected area. After getting the potential and/or salt-affected areas from image classification, different remote sensing indicators such as the Salinity Index (SI), the Normalized Differential Salinity Index (NDSI), the Normalized Vegetation Index (NDVI) and the Brightness Index (BI) were employed to study how these indices work for salt-affected areas in the study area.

### 4.6.1 Land Use Classification

Land use classification in this study was performed by digital image classification. Digital image classification is defined as the process of sorting all the image pixels into a finite number of classes or categories of data. The categorization is based on the data file values of individual pixels and it follows a set of criteria. Two major approaches are generally known: supervised and unsupervised classification. In this study Landsat 7 and ASTER data sets were used for digital image classification and visual interpretation in terms of Land Use and Saline Soil Classification.

The raw data in the six reflexive bands of the Landsat 7 data acquired on December 27, 1999 (Row 128/Path 49 and 50), were mosaicked and enhanced, as well as the raw data of the four scenes of ASTER data acquired on December 7, 2001. The selection of the False Color Composites image of Landsat 7 bands 4, 3, 2 as red, green, blue, and the False Color Composites image of ASTER bands 3, 2, 1 as red, green, blue was used for this purpose because they showed the features more distinguishable than other combinations. The False Color Composites image of Landsat 7 bands 4, 3, 2 as red, green, blue is shown in Figure 4.3, and the False Color Composite image of ASTER bands 3, 2, 1 as red, green, blue is shown in Figure 4.5.

The IsoData unsupervised classification method was run first with the maximum number of 10 classes for giving a general idea about the number of classes or categories before applying a supervised classification in the next step. The IsoData classification method calculates class means evenly distributed in the data space and then iteratively clusters the remaining pixels using the minimum distance technique. Each iteration recalculate means and reclassifies pixels with respect to the new means. This process continues until the number of pixels in each class changes by less than the selected pixel change threshold or the maximum number of iterations is reached. The results from IsoData classification from Landsat 7 and ASTER data are shown in Chapter 6.

A supervised classification was later conducted using the Maximum Likelihood Method. This method assumes that the statistics for each class in each band are normally distributed and calculates the probability that a given pixel belongs to a specific class. With this method, the study area could be classified into 6 land use classes as crops, water body, settlement, paddy fields, forest (plantation and natural), and salt-affected area respectively. The results from Maximum Likelihood classification from Landsat 7 and ASTER data are shown in Chapter 6.
The results from digital image classification were ground truth investigated in the study area in detail during field work in Thailand between October 2003 and January 2004 to observe the real land use conditions for assigning the exact position and its characteristic, and to evaluate the accuracy percent to this supervised classification.

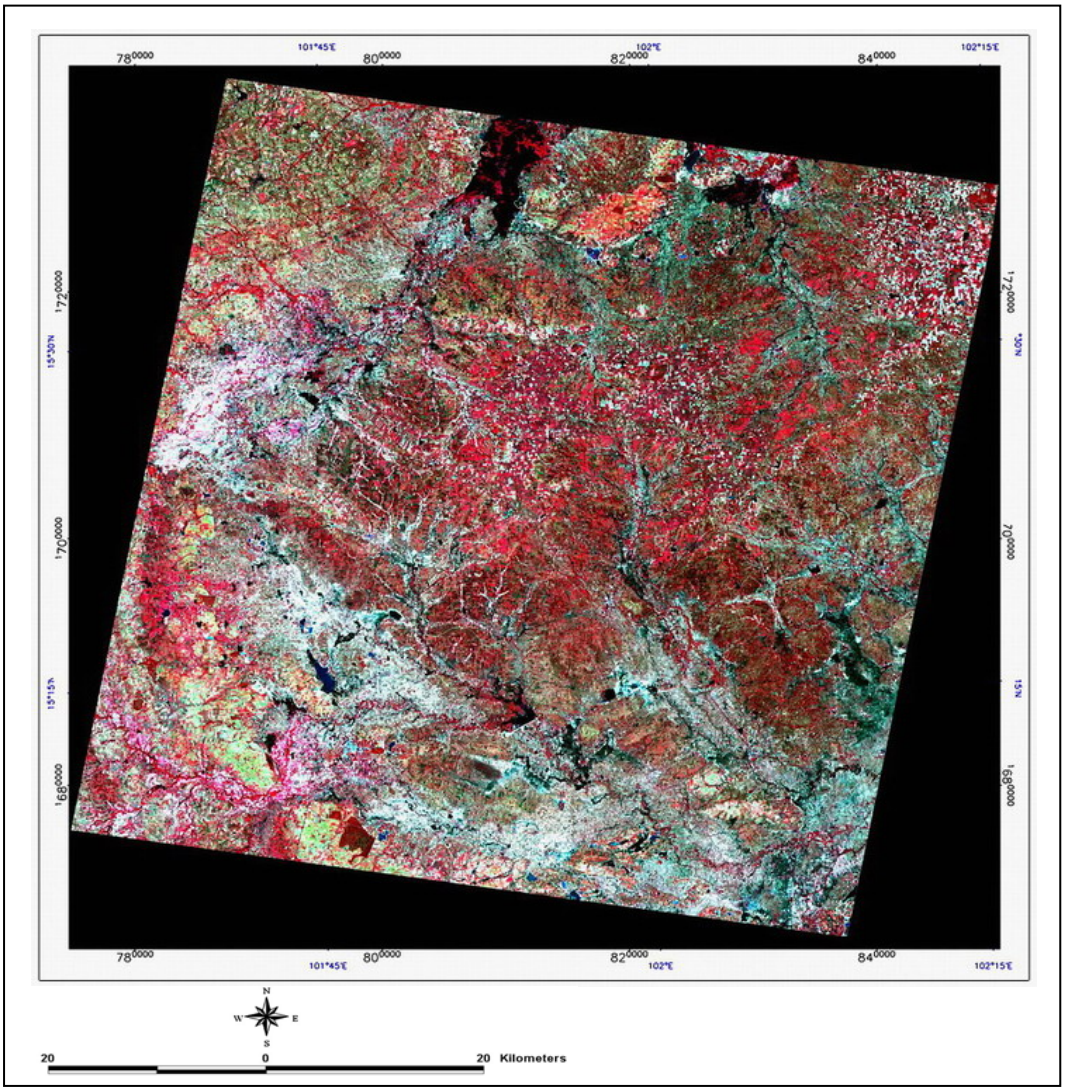


Figure 4.5 The False Color Composite image of ASTER data acquired on December 7, 2001, bands 3, 2, 1 as red, green, blue, which was used for land use classification, salinity and vegetation index analysis.

### 4.6.2 Salinity Index and Vegetation Index

Khan *et al.* (2001) used data recorded by sensor LISS-II (Linear Image Self-scanning Spectrometer) of the IRS-1B satellite in four wavebands (B1: 0.042-0.52 µm, B2: 0.52-0.59 µm, B3: 0.62-0.68 µm, and B4: 0.77-0.86 µm). These four wavebands compare and are almost equal to the wavebands of Band1, Band 2, Band 3 and Band 4 of Landsat 7 data. The comparison of spectral bands of LISS-II, Landsat 7 and ASTER sensor is shown in Table 4.4.

Table 4.4 Spectral bands and spectral ranges of LISS-II, Landsat and ASTER data.

| | LISS-II | | Landsat-TM | | ASTER | |
|---|---|---|---|---|---|---|
| | Band Number | Spectral range (µm) | Band Number | Spectral range (µm) | Band Number | Spectral range (µm) |
| VNIR | 1 | 0.42 - 0.52 | 1 | 0.45 - 0.52 | | |
| | 2 | 0.52 - 0.59 | 2 | 0.52 - 0.60 | 1 | 0.52 - 0.60 |
| | 3 | 0.62 - 0.68 | 3 | 0.63 - 0.69 | 2 | 0.63 - 0.69 |
| | 4 | 0.77 - 0.86 | 4 | 0.76 - 0.90 | 3 | 0.76 - 0.86 |
| SWIR | | | 5 | 1.55 - 1.75 | 4 | 1.60 -1.70 |
| | | | 7 | 2.08 - 2.35 | 5 | 2.145 - 2.185 |
| | | | | | 6 | 2.185 - 2.225 |
| | | | | | 7 | 2.235 - 2.285 |
| | | | | | 8 | 2.295 - 2.365 |
| | | | | | 9 | 2.360 - 2.430 |
| TIR | | | | | 10 | 8.125 - 8.475 |
| | | | | | 11 | 8.475 - 8.825 |
| | | | | | 12 | 8.925 - 9.275 |
| | | | 6 | 10.4 - 12.5 | 13 | 10.250 - 10.950 |
| | | | | | 14 | 10.950 - 11.650 |

The aim of his study was to study how the different remote sensing indices: salinity index, normalized differential salinity index, and normalized differential vegetation index and brightness index work for salt-affected soil delineation in his study area, located in the center of Punjab province of Pakistan between latitude 31o02’ to 31o45’ N and longitude 72o50’ to 73o22’E. Geologically, the soils in this area are alluvial deposits classified as silt loam, loam, and silt clay loam and loamy sands.

The indices in this study were:

*Salinity Index (SI):*

$$SI = \sqrt{B1xB3} \tag{4.1}$$

*Normalized Differential Salinity Index (NDSI):*

$$NDSI = (B3 - B4)/(B3 + B4) \tag{4.2}$$

*Brightness Index (BI):*

$$BI = \sqrt{B3^2 + B4^2} \tag{4.3}$$

Salt-affected soils are usually characterized by poorly vegetated areas and such a state of stressed vegetation could be an indirect sign of the presence of salt in the soils. The vegetation index was, therefore, included in the analysis as:

*Normalized Differential Vegetation Index (NDVI):*

$$NDVI = (B4 - B3)/(B3 + B4) \tag{4.4}$$

where B1 = 1st spectral band of LISS-II
B3 = 3rd spectral band of LISS-II
B4 = 4th spectral band of LISS-II

The results from his study showed that the indices that gave the most satisfactory results in distinguishing saline areas from non-saline areas were the Normalized Differential Salinity Index (NDSI) and the Normalized Differential Vegetation Index (NDVI). Therefore, this study adopted the Normalized Differential Salinity Index (NDSI) and the Normalized Differential Vegetation Index (NDVI), the Salinity Index (SI) and the Brightness Index (BI) and applied their equations to the data set of Landsat 7. Only the Normalized Differential Salinity Index (NDSI) and the Normalized Differential Vegetation Index (NDVI) were applied to the ASTER data set because it has similar geologically classified soil types as in the study of Khan et al. (2001).

This indices analysis is employed mosaicked Landsat 7 acquired on December 27, 1999 with Row 128/Path 49 and 50, and for the ASTER data. Only the ASTER data acquired on December 7, 2001 was chosen as the test area for this study because it showed the most sharpest contrast between salt-affected areas and non salt-affected areas by visual interpretation among other scenes and it also contains ambiguous salt-affected areas on elevated land as observed from previous digital image classification. The additional density slices and band threshold to ROI techniques were employed for enhancing the results to more easily differentiate and display the salt-affected areas from those of non salt-affected areas.

For that purpose, the data from Landsat 7 and ASTER data set were separately analyzed. The georeferencing and mosaicked of the False Color Composites image of Landsat 7 acquired on December 27, 1999, bands 4, 3, 2 as red, green, blue has been already shown in Figure 4.3 and the False Color Composites image of ASTER data of December 7, 2001, bands 3, 2, 1 as red, green, blue has also been shown in Figure 4.6.

**a) Landsat 7 Data**

For Landsat 7 data, equation 1 to 4 can be directly applied because the wavebands of the LISS-II and Landsat 7 are almost in the same range. Therefore, the indices applied on Landsat 7 data on Khorat Plateau area were:

*Salinity Index (SI):*

$$SI = \sqrt{B1xB3} \tag{4.5}$$

*Normalized Differential Salinity Index (NDSI):*

$$NDSI = (B3 - B4)/(B3 + B4) \tag{4.6}$$

*Brightness Index (BI):*

$$BI = \sqrt{B3^2 + B4^2} \tag{4.7}$$

*Normalized Differential Vegetation Index (NDVI):*

$$NDVI = (B4 - B3)/(B3 + B4) \tag{4.8}$$

where B1 = 1st spectral band of Landsat 7
B3 = 3rd spectral band of Landsat 7
B4 = 4th spectral band of Landsat 7

**b) ASTER Data**

For the ASTER data, two wavebands of LISS can be directly compared to the wavebands of ASTER as follows:

Band 3 of LISS-II ~ Band 2 of ASTER
Band 4 of LISS-II ~ Band 3 of ASTER

There are only two spectral bands of ASTER data that can compared to LISS spectral bands ranges. Therefore, the indices that can be used in this study are the Normalized Differential Salinity Index (NDSI) and the Normalized Differential Vegetation Index (NDVI), and the equations as applied to the ASTER data were modified as:

*Normalized Differential Salinity Index (NDSI):*

$$NDSI = (B2 - B3)/(B2 + B3) \tag{4.9}$$

*Normalized Differential Vegetation Index (NDVI):*

$$NDVI = (B3 - B2)/(B2 + B3) \tag{4.10}$$

where B2 = 2nd spectral band of ASTER data
B3 = 3rd spectral band of ASTER data

Results from these indices analysis and their interpretation of the Landsat 7 and ASTER are shown and later discussed in detail in Chapter 6.

## 4.7 GIS Data and Maps

For geological study and saline area mapping of the study area using the different data types in GIS a map overlay modeling has been adopted, for it simplifies association of different themes for visualization. Topographic data, previous land use maps and saline soil maps and other substantial data were digitized and integrated in order to produce new maps of saline soil and a new land use map, and to produce a GIS database. Those of supplementary GIS and geological data and its source are shown in Table 4.5. The visualization and interpretation of the different data was initially done separately for the different data types, and then for merged data sets as needed.

Table 4.5 Overview of the non-remote sensing supplementary data used in this study and its source.

| Data | Time of data acquisition | Data Format | Acquired and provided by |
|---|---|---|---|
| Soil data | 1979 | ArcView | Land Development Department (LDD) |
| Soil salinity maps | 1979 | ArcView | Land Development Department (LDD) |
| Geological maps | 1999 | Hard copy | Geological Survey Division, DMR. |